Liquid Crystals
Publication details, including instructions for authors and subscription information:
http://www.informaworld.com/smpp/title~content=t713926090

Phase behaviour of the thermotropic cubic mesogen 1,2-bis-(4- n -octyloxybenzoyl)hydrazine under pressure

Yoji Maeda[a]; Kazuya Saito[b]; Michio Sorai[b]
[a] Nanotechnology Research Institute National Institute of Advanced Industrial Science and Technology Higashi 1-1 Tsukuba, Ibaraki 305-8565 Japan, [b] Research Center for Molecular Thermodynamics, Graduate School of Science Osaka University Toyonaka, Osaka 560-0043 Japan,

Online publication date: 11 November 2010

To cite this Article Maeda, Yoji , Saito, Kazuya and Sorai, Michio(2003) 'Phase behaviour of the thermotropic cubic mesogen 1,2-bis-(4- n -octyloxybenzoyl)hydrazine under pressure', Liquid Crystals, 30: 10, 1139 — 1149
To link to this Article: DOI: 10.1080/0267829031000154354
URL: http://dx.doi.org/10.1080/0267829031000154354

LIQUID CRYSTALS, VOL. 30, NO. 10, OCTOBER, 2003, 1139–1149

Taylor & Francis
Taylor & Francis Group

Phase behaviour of the thermotropic cubic mesogen 1,2-bis-(4-*n*-octyloxybenzoyl)hydrazine under pressure

YOJI MAEDA*

Nanotechnology Research Institute, National Institute of Advanced Industrial Science and Technology, Higashi 1-1, Tsukuba, Ibaraki 305-8565, Japan

KAZUYA SAITO and MICHIO SORAI

Research Center for Molecular Thermodynamics, Graduate School of Science, Osaka University, Toyonaka, Osaka 560-0043, Japan

(*Received 30 January 2003; accepted 24 April 2003*)

The phase transition behaviour of an optically isotropic, thermotropic cubic mesogen 1,2-bis-(4-*n*-octyloxybenzoyl)hydrazine, BABH(8), was investigated under pressures up to 200 MPa using a high pressure differential thermal analyser, wide-angle X-ray diffraction and a polarizing optical microscope equipped with a high pressure optical cell. The phase transition sequence, low temperature crystal (Cr_2)–high temperature crystal (Cr_1) – cubic (Cub)–smectic C (SmC)–isotropic liquid (I) observed at atmospheric pressure, is seen in the low pressure region below about 30 MPa. The cubic phase disappears at high pressures above 30–40 MPa, in conjunction with the disappearance of the Cr_1 phase. The transition sequence changes to Cr_2–SmC–I in the high pressure region. Since only the Cub–SmC transition line among all the phase boundaries has a negative slope (dT/dP) in the temperature–pressure phase diagram, the temperature range for the cubic phase decreases rapidly with increasing pressure. As a result, a triple point was estimated approximately as 31.6 ± 2.0 MPa, 147.0 ± 1.0°C for the SmC, Cub and Cr_1 phases, indicating the upper limit of pressure for the observation of the cubic phase. Reversible changes in structure and optical texture between the Cub and SmC phases were observed from a spot-like X-ray pattern and dark field for the cubic phase to the Debye–Sherrer pattern and sand-like texture for the SmC phase both in isobaric and isothermal experiments.

1. Introduction

The study of thermotropic cubic liquid crystalline phases began in 1957, when Gray *et al.* [1] published the synthesis of 4′-*n*-hexadecyloxy- and 4′-*n*-octadecyloxy-3′-nitrobiphenyl-4-carboxylic acid: referred to as ANBC(16) and ANBC(18), respectively. A number of thermotropic cubic mesogens have now been reported [2]. The majority of these compounds are carbohydrates and polycatenar compounds including several examples of metallomesogens. In 1978, the 1,2-bis-(4-*n*-alkyloxybenzoyl)hydrazines, denoted BABH(*n*), where *n* indicated the number of carbon atoms in the alkoxy chain, were synthesized by Schubert *et al.* [3]. The BABH(*n*) compounds are examples of classical thermotropic mesogens and the chemical structure of 1,2-bis-(4-*n*-octyloxybenzoyl)-hydrazine BABH(8) is,

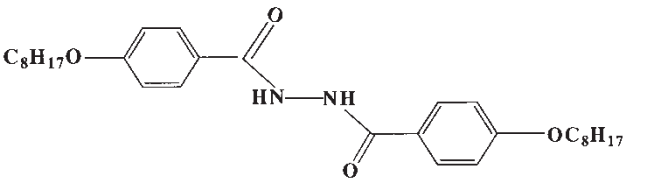

As reported by Demus *et al.* [4], the octyloxy-, nonyloxy- and decyloxy-homologues of the BABH(*n*) series exhibit both cubic (Cub) and smectic C (SmC) phases, and show the phase sequence crystal (Cr_I)–crystal (Cr_{II})–Cub–SmC–isotropic liquid (I). Interestingly, the order of phases (Cub–SmC) is reversed in comparison to that (SmC–Cub) found for ANBC(*n*). Göring *et al.* [5] determined the crystal structure of BABH(8) as well as the structures of the cubic and SmC phases. BABH(8) crystallizes in a triclinic cell with the space group $P\bar{1}$ (the dimensions of the unit cell are

*Author for correspondence; e-mail: yoji.maeda@aist.go.jp

Liquid Crystals ISSN 0267-8292 print/ISSN 1366-5855 online © 2003 Taylor & Francis Ltd
http://www.tandf.co.uk/journals
DOI: 10.1080/0267829031000154354

$a = 0.4987$ nm, $b = 1.1549$ nm, $c = 1.3466$ nm, $\alpha = 112.23°$, $\beta = 94.27°$, and $\gamma = 95.10°$). The molecules in the crystalline phase form sheets linked by hydrogen bonds. The cubic phase has a body centred cubic cell ($a = 6.46$ nm) with a space group *Ia3d*. The jointed-rod model for the *Ia3d* space group, i.e. two interwoven, but unconnected, networks of rods linked three by three, was proposed for the cubic phase of BABH(8) [6–10]. The precise calorimetric measurements on BABH(8) were carried out by Sorai and his collaborators [11], and provide reliable thermodynamic quantities of the phase transitions. Saito *et al*. [12, 13] discussed the phase diagrams of several cubic liquid crystalline compounds in terms of the number of carbon atoms in the alkyl moieties.

One of the authors (Y.M.) studied the phase behaviour of the ANBC(*n*) homologous series under hydrostatic pressure using high pressure differential thermal analysis (DTA), and determined the *T* vs. *P* phase diagram in the heating and cooling modes [14, 15]. As already reported by Demus *et al*. [4], the phase sequence of BABH(8) is: low temperature crystal (Cr_2)→high temperature crystal (Cr_1)→Cub→SmC→I. In BABH(8) the cubic phase is located on the low temperature side of the SmC phase, while the cubic phase of ANBC(*n*) appears on the high temperature side. This inversion in phase sequence for BABH(*n*) and ANBC(*n*) prompted us to investigate the phase behaviour of BABH(8) under hydrostatic pressure, with particular focus on the effect of pressure on the phase stability of the cubic phase.

In this paper, we present the experimental results of the thermal, morphological and structural behaviour of BABH(8) under hydrostatic pressures up to 200 MPa using a high pressure DTA, a polarizing optical microscope equipped with a high pressure optical cell, and a wide angle X-ray diffraction (WAXD) system equipped with a high pressure vessel.

2. Experimental

2.1. *Sample characterization under ambient pressure*

BABH(8), prepared as described in [11], was used in this study. Samples had been recrystallized from ethanol several times and the purity was confirmed by infrared (IR), ^{1}H NMR and mass spectroscopies, and elemental analysis. Thermal characterization of BABH(8) was performed on Perkin–Elmer DSC-7 and MacScience DSC-3001 calorimeters at a scanning rate of $5°C\,min^{-1}$ under N_2 gas flow. Temperatures and heats of transition were calibrated using standard materials (indium and tin). Transition temperatures were determined as the onset of the transition peaks at which the tangential line of the inflection point of the rising part of the peak crosses over the extrapolated baseline. Morphological characterization was performed using a Leitz Orthoplan polarizing optical microscope (POM) equipped with a Mettler hot stage FP-82.

2.2. *DTA measurements under pressure*

The high pressure DTA apparatus used in this study is described elsewhere [16]. The DTA system was operated in a temperature region between room temperature and 250°C under hydrostatic pressures up to 200 MPa. Dimethylsilicone oil with a medium viscosity (100 cSt) was used as the pressurizing medium. The sample weighing about 4 mg was put in the sample cell and coated with epoxy adhesives, in order to fix it in the bottom of the cell and also to prevent direct contact with the silicone oil. A new aliquot of BABH(8) was used for each DTA measurement. The DTA runs were performed at a constant scanning rate of $5°C\,min^{-1}$ under various pressures. Peak temperatures were taken as the transition temperatures for constructing the real temperature vs. pressure phase diagram. When estimating a specific point, such as a triple point, the transition temperature was corrected to become the onset temperature by subtracting a temperature difference between the onset and peak temperatures, of approximately 3–4°C. The enthalpy changes at the phase transitions of BABH(8) were determined by comparison with the fusion enthalpy of indium ($28.5\,J\,g^{-1}$ and assuming constant value, irrespective of pressure) under the same pressures.

2.3. *Morphological and X-ray characterization under pressure*

The optical texture observation of BABH(8) under hydrostatic pressure was performed using a Leitz Orthoplan POM equipped with a high pressure optical cell system [17]. Transmitted light intensity through the POM with crossed Nicols was measured using a Mettler FP-90 photomonitor under atmospheric and hydrostatic pressures. Pressure and temperature were monitored simultaneously during the morphological observation. The texture observation was performed during both heating and cooling processes under isobaric conditions and during pressure changes under isothermal conditions in the pressure range up to 50 MPa.

Structural changes during the phase transitions of BABH(8) under pressure were observed using a high pressure wide angle X-ray diffraction (WAXD) apparatus [16]. The high pressure vessel was set on the wide angle goniometer of a 12 kW rotating anode X-ray generator (Rotaflex RU200, Rigaku Co.). The sample was inserted into the vertical hole of the beryllium spindle as the sample cell. The beryllium spindle was mechanically compressed for pressure sealing using upper and lower pressure blocks. Then the sample was pressurized hydrostatically at pressures up to 200 MPa. A Ni-filtered Cu K_α X-ray beam was used to irradiate the sample, and diffraction patterns were obtained using

an imaging plate detector (BAS-IP $127 \times 127\,mm^2$, Fuji Photo Film Co.).

3. Results and discussion

It is known that BABH(8) shows the $Cr_2 \leftrightarrow Cr_1 \leftrightarrow$ Cub$\leftrightarrow$SmC$\leftrightarrow$I transition sequence at atmospheric pressure [2–5]. On heating, the Cr_2–Cr_1 and Cr_1–Cub transitions occur at 130.0 and 133.4°C, respectively. The cubic phase extended over a relatively wide temperature range of about 20°C, and then a small peak associated with the Cub–SmC transition was observed at 153.7°C. Finally a sharp peak arising from the SmC–I transition appeared at 163.4°C. Table 1 lists the thermodynamic quantities associated with the phase transitions of BABH(8), determined in the present study. Figure 1 shows the POM photographs of the textures of BABH(8) observed on cooling from the isotropic liquid at 175°C under atmospheric pressure. Figure 1 (*a*) shows the dark field of the isotropic liquid under crossed polarisers at 170°C. The sand-like texture of the SmC phase appears at 166°C, figure 1 (*b*). The sand-like texture is observed at temperatures up to about 160°C, 1 (*c*), and then the texture disappears, being replaced by the dark field of the cubic phase at 159°C, figure 1 (*d*). The optically isotropic dark field of the cubic phase was observed in the temperature region between 159 and 125°C. Finally the Cub–Cr_1 transition (crystallization) occurs at about 125°C, figure 1 (*e*). The spherulitic texture of the Cr_2 crystals is observed at 30°C, figure 1 (*f*). Thus clear changes in texture are observed reversibly during the I–SmC–Cub–Cr_1–Cr_2 transition sequence under atmospheric pressure. The POM-transmitted light intensity vs. temperature curves of BABH(8) also revealed clear reversible changes in texture in the cooling and subsequent heating processes.

3.1. *Thermal behaviour under pressure*

The thermal behaviour of BABH(8) was investigated under hydrostatic pressure to study the effect of pressure on the thermal stability of the cubic and SmC phases. Figure 2 shows the heating and subsequent cooling curves of BABH(8) at 10 MPa. The DTA heating curve at 10 MPa showed a double peak corresponding to the $Cr_2 \rightarrow Cr_1$ and $Cr_1 \rightarrow$Cub transitions at 136.4 and 139.8°C, respectively, a very small peak for the Cub$\rightarrow$SmC transition at 153.5°C, and a small peak for the SmC$\rightarrow$I transition at 166.8°C. The subsequent cooling process showed a rather noisy curve, but the I$\rightarrow$SmC$\rightarrow$Cub$\rightarrow Cr_1 \rightarrow Cr_2$ transitions were seen at 10 MPa. The DTA curves at 10 MPa exhibited essentially the same transition behaviour as those recorded under atmospheric pressure, indicating the reversible nature of the phase transitions, $Cr_2 \leftrightarrow Cr_1 \leftrightarrow$Cub$\leftrightarrow$SmC$\leftrightarrow$I.

Figure 3 compares the DTA heating curves of BABH(8) at 10, 30, and 50 MPa. All three curves show clearly a main peak due to the melting of the crystal and a small peak due to the SmC$\rightarrow$I transition at high temperatures. It is noted here that the Cub$\rightarrow$SmC transition peak is observed at 10 MPa, but is absent at higher pressures. In fact, the Cub$\rightarrow$SmC transition was observed only in the very low pressure region below 10–12 MPa. By contrast, the double peak corresponding to the $Cr_2 \rightarrow Cr_1$ and $Cr_1 \rightarrow$Cub transitions was observed at pressures up to 30 MPa, but merged into a single peak, suggesting the disappearance of the Cr_1 phase, in the high pressure range. Figure 4 shows the DTA heating curves of BABH(8) at 70, 104, 149, and 192 MPa. All the DTA curves simply show two peaks corresponding to melting and isotropization. In the high pressure region the transition sequence is expressed as Cr$\rightarrow$mesophase$\rightarrow$I on heating.

Figure 5 shows the temperature–pressure phase diagrams of BABH(8) obtained on heating and cooling under pressures up to 200 MPa. Open and filled symbols are the data obtained on heating and cooling, respectively. The phase diagram derived from the heating mode shows the thermodynamically stable phases in the whole pressure region. The transition curves obtained on heating can be expressed approximately as either first or second order polynomials in terms of pressure:

(t/°C: peak temperature)

Transition	*0 < P < 30–40 MPa*
$Cr_2 \rightarrow Cr_1$	$t/°C = 134.5 + 0.487_9$ (P/MPa)
$Cr_1 \rightarrow$Cub	$t/°C = 137.5 + 0.420_1$ (P/MPa)
Cub$\rightarrow$SmC	$t/°C = 155.6 - 0.151_6$ (P/MPa)
	30–40 MPa < P
$Cr_2 \rightarrow$SmC	$t/°C = 141.7 + 0.297_6$ (P/MPa)
	Whole pressure range
SmC$\rightarrow$I	$t/°C = 165.5 + 0.397_5$ (P/MPa) $- 5.110_6 \times 10^{-4}$ (P/MPa)^2.

Table 1. Thermodynamic quantities associated with the phase transitions of BABH(8).

Phase transition	T/°C	ΔH/kJ mol^{-1}	ΔS/J K^{-1} mol^{-1}	$(dt/dP)_{1atm}$	ΔV/cm^3 mol^{-1}
Cr$\rightarrow$Cub	133.5	51.8	127.4	0.420_1	53.5_2
Cub$\rightarrow$SmC	153.7	1.34	3.1	-0.151_6	-0.4_7
SmC$\rightarrow$I	163.4	7.17	16.4	0.464_1	7.6_1

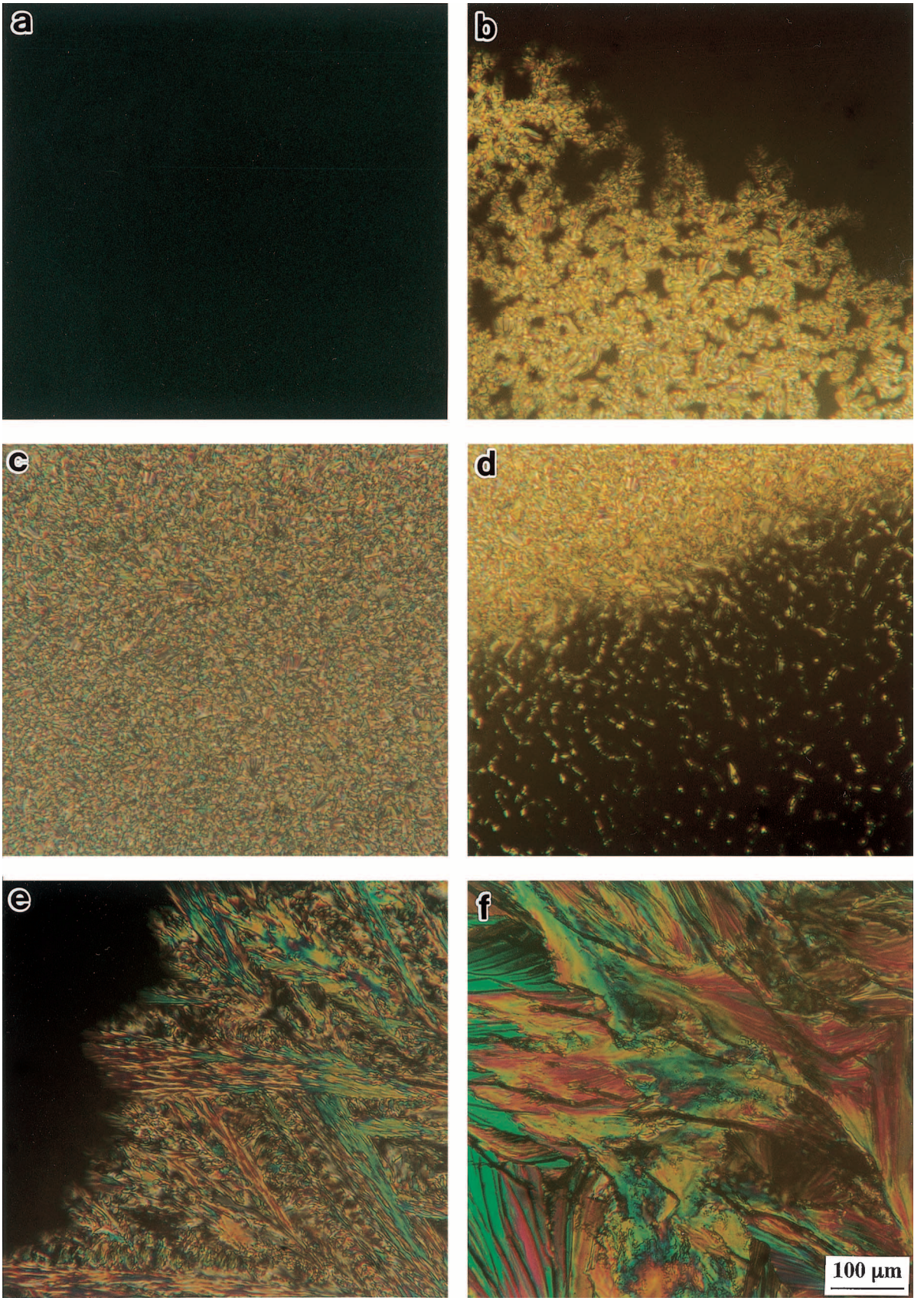

Figure 1. POM photographs of BABH(8) on cooling from the isotropic liquid under atmospheric pressure: (*a*) isotropic liquid at 170°C; (*b*) I→SmC transition at 166°C; (*c*) SmC phase at 165°C; (*d*) SmC→Cub transition at 159°C; (*e*) Cub→Cr_1 transition at 125°C; (*f*) Cr_2 at 30°C.

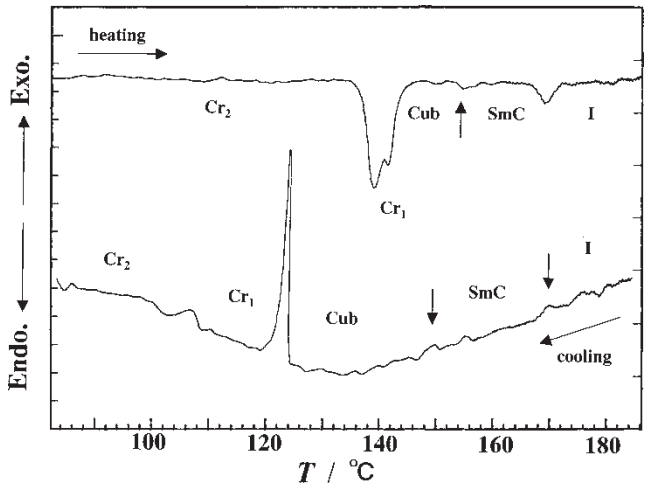

Figure 2. DTA curves of BABH(8) at 10 MPa. Scanning rate: 5°C min^{-1}.

Here it should be noted that the Cub→SmC transition line has a negative slope in the T vs. P phase diagram. Since the Cr_1→Cub and Cub→SmC transition lines have positive and negative slopes (dT/dP) respectively, the cubic phase is observed disappear under high pressure. The triple point for the Cr_1, Cub, and SmC phases was estimated to be approximately 31.6 ± 2.0 MPa, 147.0 ± 1.0°C; this is only approximate because there are only few available data and those are relatively scattered, corresponding to the Cub–SmC transition in the very low pressure region. Similarly, one would expect an intersection between the Cr_2–Cr_1 and Cr_1–Cub transition lines, and another between the Cr_2–Cr_1 and Cr_2–SmC transition lines, resulting in the hypothetical triple points at 44.2 MPa and 34.3 MPa, respectively. The former point is not seen within

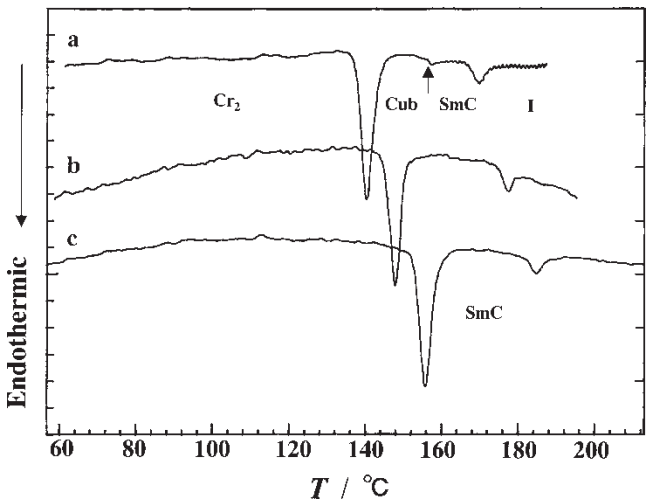

Figure 3. DTA heating curves of BABH(8) at (*a*) 10, (*b*) 30, (*c*) 50 MPa. Heating rate: 5°C min^{-1}.

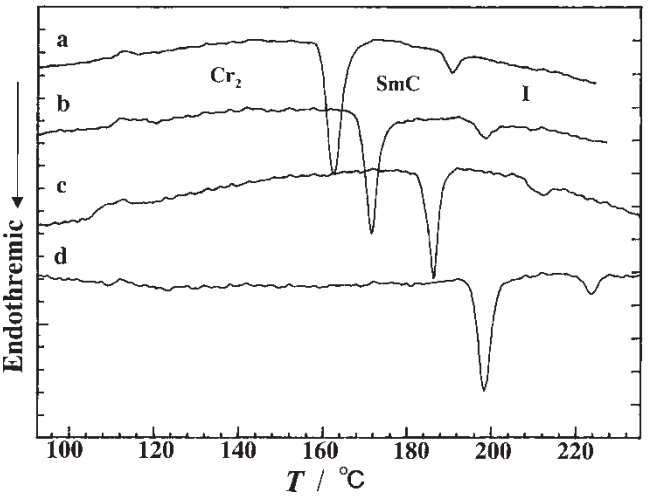

Figure 4. DTA heating curves of BABH(8) at (*a*) 70, (*b*) 104, (*c*) 150, (*d*) 192 MPa. Heating rate: 5°C min^{-1}.

experimental error and should be rejected. On the other hand, the latter point of 34.3 MPa, c.148.2°C should exist as the triple point for the Cr_2, Cr_1 and SmC phases, indicating the upper limit of pressure for the Cr_1 phase. There are two triple points in the pressure region between 30 and 35 MPa. This implies a very short Cr_1–SmC phase boundary between the two

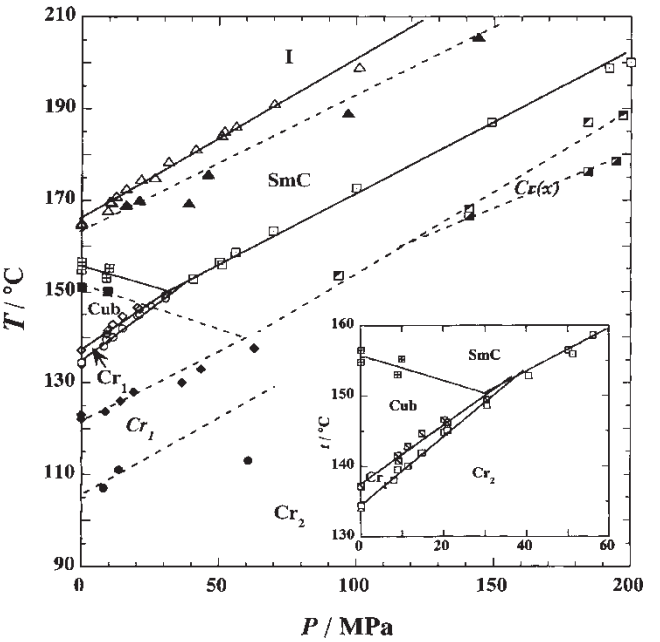

Figure 5. Temperature vs. pressure phase diagrams of BABH(8) constructed in the heating and cooling modes. Open symbols and solid curves are the data and transition lines observed on heating, while filled symbols and broken curves are the data and transition lines obtained on cooling.

triple points that cannot be resolved, because the two triple points are too close together. Since the cubic phase disappears under high pressure, the mesophase in the high pressure region can be identified as the SmC phase. It is interesting to note that the temperature range for the SmC phase is approximately constant at about 30°C, irrespective of pressure up to 200 MPa.

From the thermodynamic data in table 1 and the (dT/dP) obtained by high pressure DTA, the volume change at the phase transition can be estimated using the Clausius–Clapeyron equation $dT/dP = \Delta V/\Delta S = T\Delta V/\Delta H$. Since the Cub–SmC transition has a negative slope (dT/dP) and positive enthalpy of transition ΔH, the volume change is assigned as negative, i.e., ΔV ($\equiv V_{SmC} - V_{Cub}$) < 0. This means that the molar volume of the SmC phase at higher temperatures is smaller than that of the low temperature cubic phase, i.e. $V_{SmC} < V_{Cub}$. In the case of ANBC(16) having the inverse phase sequence [14, 15], both the slope (dT/dP) and the enthalpy of transition for the SmC→Cub transition are positive. Thus the same relationship $V_{SmC} < V_{Cub}$ holds for the SmC→Cub transition for ANBC(16). This suggests that the net volume of the cubic phase is primarily determined not by the highly disordered alkyl chains but by the densely packed and three-dimensionally connected TPMS (triply periodic minimal surface, one of infinitely periodic minimal surface) structure, according to the model of the cubic phase proposed by Saito and Sorai [18]. This should be an important factor that brings about the larger entropy of alkyl chains in the cubic phase than the SmC [19, 20] because the chain entropy strongly depends on the available (free) volume of chains.

It was found that the DTA cooling curves of BABH(8) clearly showed double peaks during the SmC→Cr_2 transition under high pressures above 100 MPa, and that the temperature difference between the two peaks becomes larger with increasing pressure. Figure 6 shows the thermal behaviour of BABH(8) on heating and subsequent cooling at 192 MPa. One can see clearly the appearance of a pressure-induced crystalline phase Cr(x) between the two peaks in the cooling process. Since the Cr(x) phase does not appear in the heating process under the same pressure, the pressure-induced crystalline phase is metastable. The Cr(x) phase is considered to be different from the Cr_1 phase that appears in the low pressure region, as shown in figure 2. The pressure-induced crystalline phase has not to date been characterized.

We attempted to estimate the transition enthalpies for the transitions under pressure using a general procedure for the estimation of transition enthalpy based on heat-flux DSC. Before doing this, we measured the enthalpy of fusion for indium at various pressures and

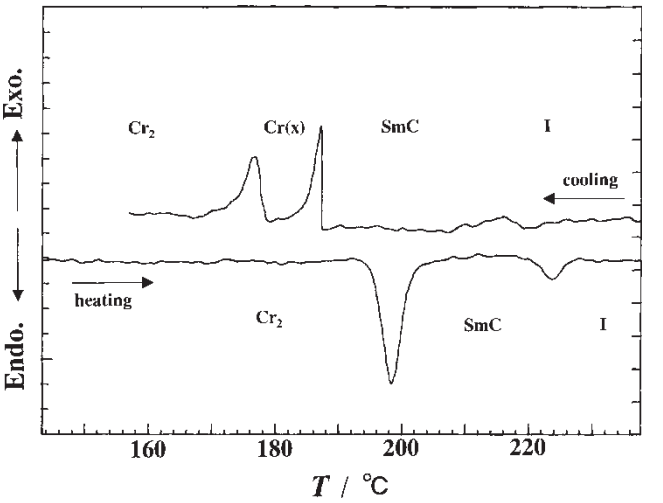

Figure 6. DTA heating and subsequent cooling curves of BABH(8) at 195 MPa. Scanning rate: 5°C min^{-1}.

then constructed a calibration curve for the standard value ΔH of indium as the apparatus constant depending on pressure. Figure 7 shows the pressure dependence of the calculated transition enthalpies for the Cr–Cub, Cub–SmC and SmC–I transitions in the low pressure region, and also the Cr_2–SmC and SmC–I transitions in the high pressure region. For convenience, the transition enthalpies for the Cr_2–Cr_1 and Cr_1–Cub transitions were combined into a single transition enthalpy of the Cr–Cub transition in the low pressure

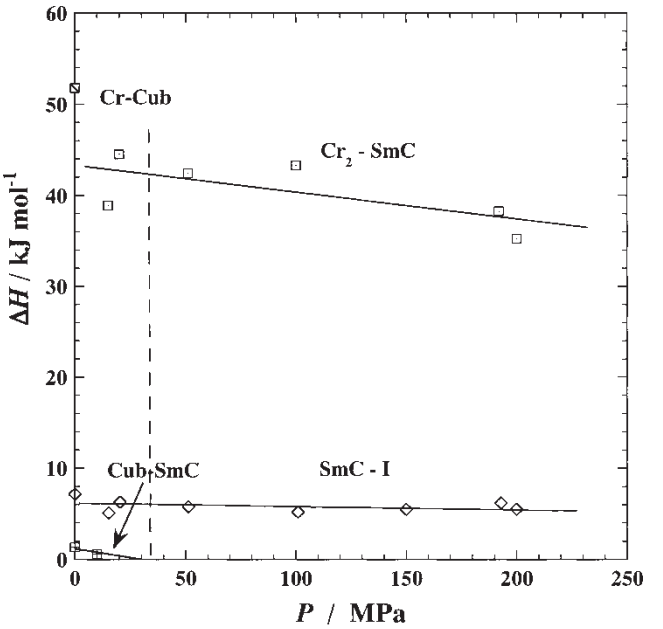

Figure 7. Pressure dependence of the transition enthalpies for the Cr–Cub, Cub–SmC, Cr_2–SmC and SmC–I transitions in the pressure region up to 200 MPa.

region. The corresponding entropies of transitions are shown in figure 8. It is noted that the enthalpy and entropy data for the Cr–Cub transition in the low pressure region fall on the same line as the Cr_2–SmC transition data in the high pressure region.

The Cub–SmC transition enthalpy is very small and decreases with pressure, disappearing completely at about 30 MPa. It is noted that this is not necessary for the disappearance of the cubic phase from the temperature–pressure diagram. The entropy of the Cub–SmC transition consists of two competing contributions as shown in previous papers [19, 20]. One contribution arises from the mesogenic cores and can be assigned to the formation of the higher order cubic structure from the layered aggregation [18]. Since our microscopic understanding of this contribution is rather unclear, it would be unwise to speculate on the possible effects of pressure on this contribution. The other contribution to the entropy of transition is from the alkyl chains. As the entropy of transition is the difference in entropies of two phases, a comparison of pressure effects on each phase is necessary. The chain contribution is negative as revealed by the decrease in the entropy of transition upon elongating the alkyl chain [4]. This means that the chain entropy is smaller in the SmC phase than in the cubic phase. Considering the stiffness of the cubic phase of ANBC [21, 22], BABH is expected to be more compressed in the SmC phase than in the cubic phase. As the available volume is an important factor in determining the entropy of alkyl chains, the entropy difference between the chains will increase, resulting in the reduced magnitude of the entropy of transition. On the other hand, the number of methylene groups that serve as an intramolecular solvent ('self-solvent') [23, 24] may decrease with increasing pressure, leading to a possible increase in the entropy of transition. The decrease in the entropy of transition experimentally observed in this study suggests that the former effect dominates.

The ΔH and ΔS for the Cr_2–SmC transition decrease linearly (from 110 to 80 $J\,K^{-1}\,mol^{-1}$ in terms of entropy) with increasing pressure, while those for the SmC–I transition are almost constant (13–15 $J\,K^{-1}\,mol^{-1}$), and independent of pressure. The decrease of the entropy of melting (Cr→Cub or SmC phase) is due to the reduced free volume of alkyl chains whereas the almost constant value for the SmC–I transition suggests that the decrease in entropy by compression works equally in both phases.

3.2. *Morphological and structural observations under pressure*

Figure 9 shows the change in POM-transmitted light intensity for BABH(8) on heating and subsequent cooling at 10 MPa. One can easily locate the reversible changes in textures associated with the Cr_2–Cr_1, Cr_1–Cub, Cub–SmC and SmC–I transitions of BABH(8). It is noted that the optically isotropic cubic and liquid phases under pressure show relatively strong intensities because the dark brown field, rather than a black field

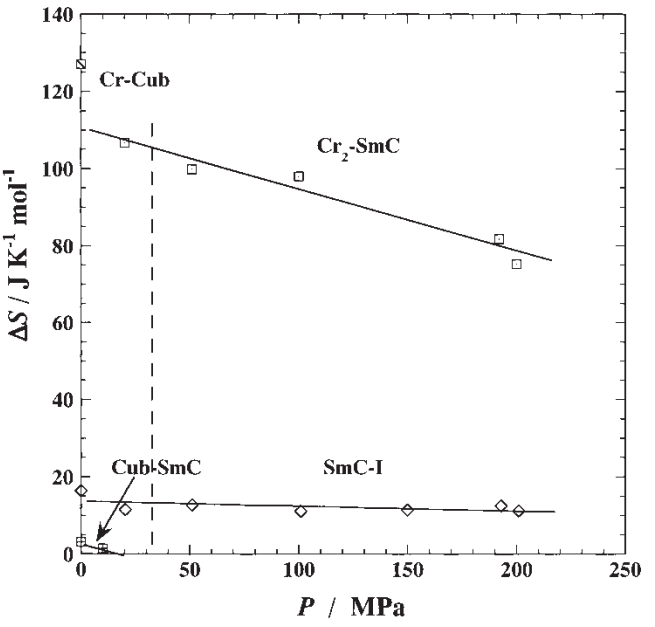

Figure 8. Pressure dependence of the transition entropies for the Cr–Cub, Cub–SmC, Cr_2–SmC and SmC–I transitions.

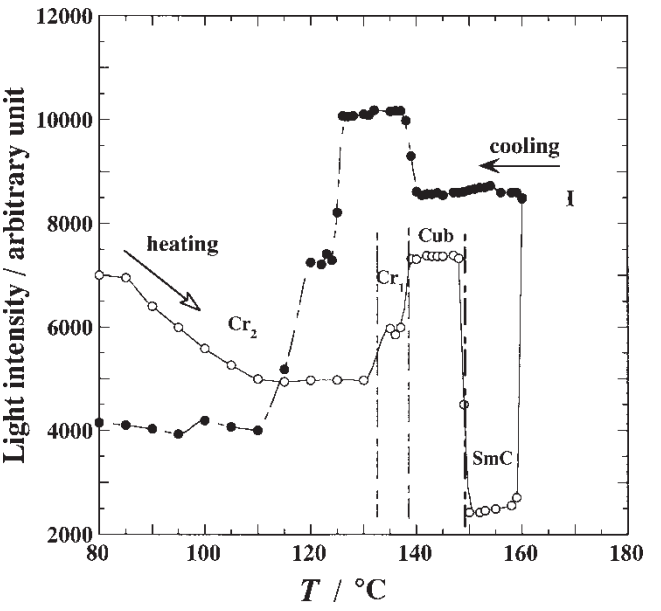

Figure 9. POM-transmitted light intensity vs. temperature curves of BABH(8) on heating (open symbols) and cooling (filled symbols) at 10 MPa.

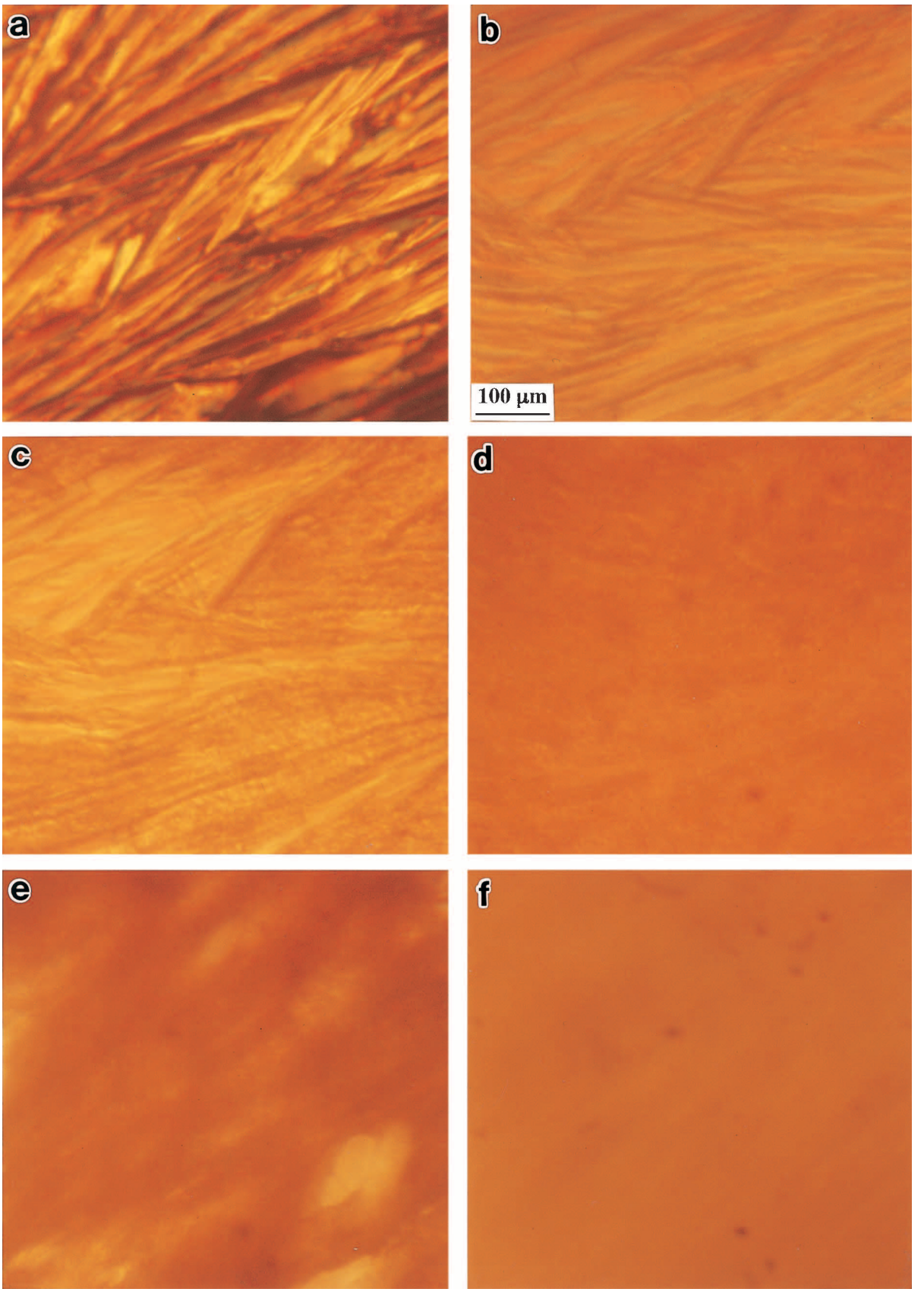

Figure 10. POM photographs of the textures of BABH(8) on heating at 50 MPa: (*a*) Cr_2 at 25°C, 1 atm; (*b*) Cr_2 at 25°C; (*c*) Cr_2 at 100°C; (*d*) SmC phase at 155°C; (*e*) SmC phase at 170°C; (*e*) isotropic liquid at 185°C.

as seen under atmospheric pressure, is observed under hydrostatic pressure. The textures observed at 10 MPa are basically the same as those observed under atmospheric pressure. The POM-transmitted light intensity vs. temperature curves on heating and subsequent cooling at 15 MPa are essentially the same as those at 10 MPa, except for the very narrow temperature range of the cubic phase. Figures 10 and 11 show the textures of BABH(8) observed on heating, and the POM-transmitted light intensity vs. temperature curves at 50 MPa, respectively. The disappearance of the cubic phase is confirmed by the texture observations and transmitted light intensity measurements under high pressures, which is in accord with the high pressure DTA results described in the last section. Thus the Cr_2–SmC–I transition occurs reversibly at 50 MPa and higher pressures.

Figure 12 shows the effect of pressure on the texture (i.e. dark brown field) of the optically isotropic cubic phase isothermally at 145°C. When the pressure is raised from 5 to 10 MPa, the dark brown field of the cubic phase at 5 MPa, figure 12 (*a*), changes to a sea-island texture of partly dark field and partly sand-like textures of the SmC phase, figure 12 (*b*). On increasing the pressure further to 20 MPa, the texture changes completely to the sand-like texture of the SmC phase, figure 12 (*c*). The change between the dark field and sand-like texture is reversible at 145°C, depending on the applied pressure. This exhibits the reversible Cub–SmC transition under isothermal conditions, similar to the Cub–SmC transition on heating and cooling at

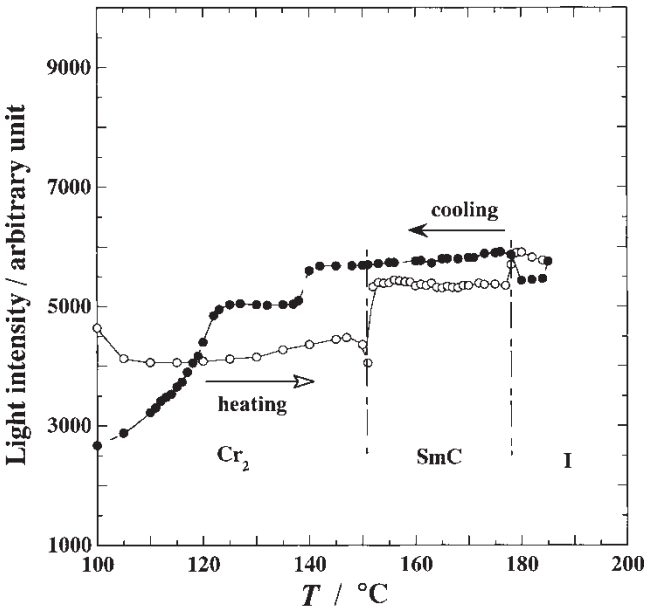

Figure 11. POM-transmitted light intensity vs. temperature curves of BABH(8) on heating (open symbols) and cooling (filled symbols) at 50 MPa.

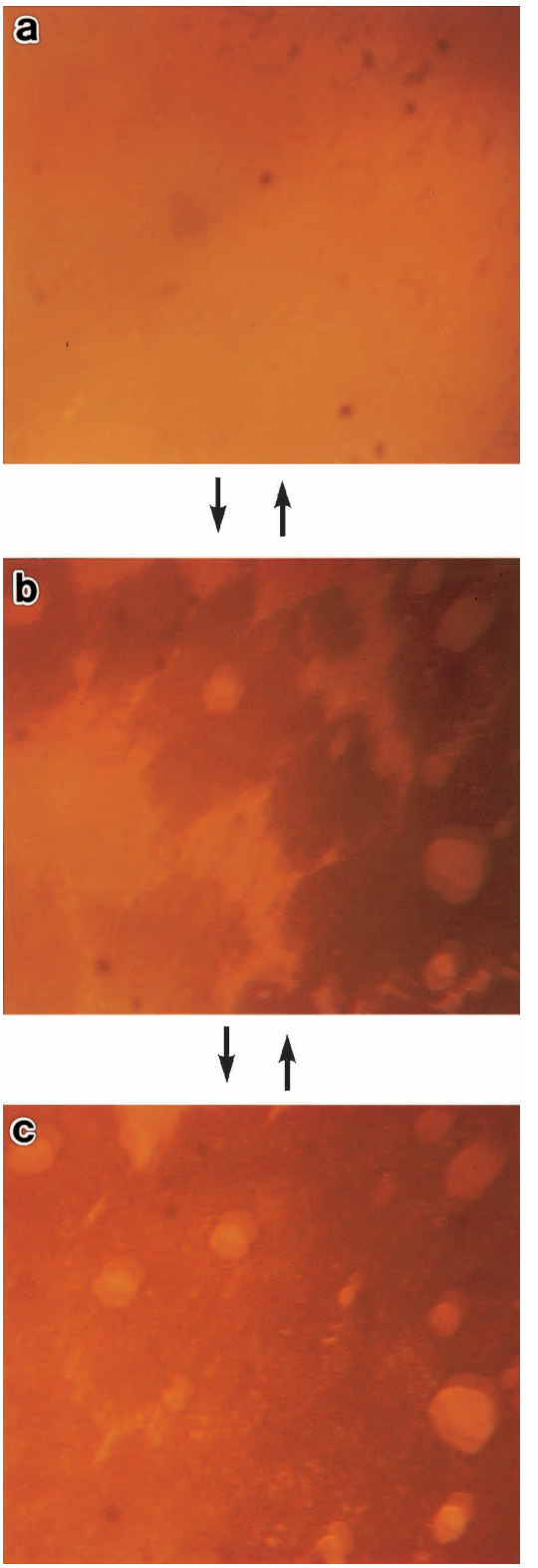

Figure 12. POM photographs of the reversible change in texture between the Cub and SmC phases of BABH(8) on pressurizing and subsequent depressurizing processes at 145°C: (*a*) Cub phase at 5 MPa; (*b*) Cub→SmC transition at 10 MPa; (*c*) SmC phase at 20 MPa.

10 MPa. The texture change during the Cub–SmC transition was also found at 130°C under higher pressures between 20 and 25 MPa. The phenomenon supports the negative slope (dT/dP) of the Cub–SmC transition line in the phase diagram shown in figure 5.

Figure 13 shows the X-ray diffraction patterns of the crystalline (Cr_2) phase of a fresh sample at room temperature and atmospheric pressure, the cubic phase at 135°C and 1 MPa, the SmC phase at 165°C and 25 MPa, and the SmC phase at 181°C and 100 MPa. The X-ray pattern of the original Cr_2 crystal (*a*) shows a spotty Debye–Sherrer pattern, indicating the crystals being single crystal-like. The spot-like pattern (*b*) for the cubic phase at 135°C and 1 MPa is similar to that of the cubic phase of an oriented sample reported by Göring *et al.* who presented reliable results on a monodomain sample [5]. Table 2 lists the values of the *d* spacing estimated from the X-ray patterns of the Cr_2, Cub and SmC phases. Several low angle peaks for the cubic phase are due to the reflection from the {2 1 1} plane at $2\theta = 3.18°$ ($d = 2.77$ nm) and other reflections. The {0 0 1} reflection of the SmC phase at 165°C and 25 MPa, figure 13 (*c*), is observed at $2\theta \cong 3.5°$ ($d =$ 2.54 nm). This reflection is close to the lower peak for the cubic phase. The X-ray pattern of the SmC phase at 181°C and 100 MPa, figure 13 (*d*), is the same as that of the SmC phase at 165°C and 25 MPa. The mesophase in the high pressure region is confirmed structurally as the SmC phase. The phase transition between the cubic and SmC phases was easily observed by analysing the X-ray patterns.

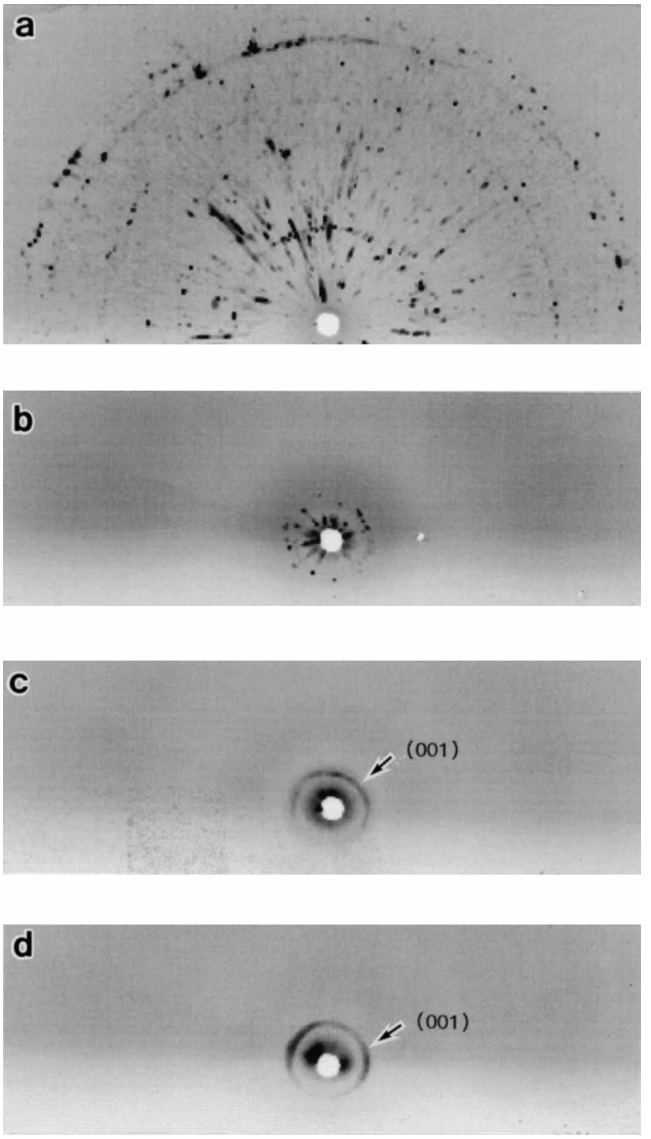

Figure 13. X-ray diffraction patterns of (*a*) fresh sample (Cr_2) of BABH(8) at 25°C and atmospheric pressure; (*b*) the cubic phase at 135°C and 1 MPa; (*c*) the SmC phase at 165°C and 25 MPa; (*d*) the SmC phase at 181°C and 100 MPa.

4. Conclusion

The phase transition behaviour of BABH(8) was investigated under hydrostatic pressures up to 200 MPa using a high pressure DTA, a polarizing optical microscope equipped with a high pressure optical cell, and WAXD equipped with a high pressure vessel. The temperature versus pressure phase diagram was constructed. The phase sequence for BABH(8) may be summarized thus: the phase transition sequence occurs reversibly via $Cr_2 \leftrightarrow Cr_1 \leftrightarrow Cub \leftrightarrow SmC \leftrightarrow I$ in the low pressure region below 20 MPa; the sequence $Cr_2 \leftrightarrow SmC \leftrightarrow I$ is seen in the pressure region between 30 and 100 MPa; and the sequence becomes $Cr_2 \rightarrow SmC \leftrightarrow I$ under higher pressures. It can be seen in the phase diagram

Table 2. *d* spacing calculated from the X-ray reflections of the Cr_2, cubic and SmC phases of BABH(8).

d spacing/nm (2θ/°)		
Cr_2 25°C	Cubic 150°C	SmC 161°C
	2.77 (3.18)	
	2.63 (3.36)	
	2.51 (3.51)	
	2.41 (3.66)	2.54 (3.48)
2.10 (4.20)		
1.55 (5.70)		
1.02 (8.70)		
0.72 (12.2)		
0.60 (14.7)		
0.58 (15.3)		
0.47 (19.0)		
0.38 (23.5)		
0.36 (24.6)		
0.35 (25.4)		

that the Cub→SmC transition line has a negative slope and that the transition line crosses with the Cr_1→Cub transition line. The cubic phase apparently disappears at about 20 MPa, giving a triple point for the Cr_1, Cub and SmC phases at 31.6 ± 2.0 MPa and 147.0 ± 1.0°C. The Cub→SmC transition was observed using POM and WAXD techniques. The dark brown field for the optically isotropic cubic phase changed reversibly to the sand-like texture of the SmC phase both on isobaric and isothermal scans. The spot-like diffraction pattern of the cubic phase at 1–5 MPa changed to the Debye–Sherrer ring pattern of the SmC phase at 30–40 MPa in isothermal measurements between 130 and 145°C. Thus has been confirmed experimentally that the Cub–SmC transition is reversible and thermodynamically first order.

K.S. and M.S. are grateful for financial support from the Ministry of Education, Culture, Sports, Science, and Technology, Japan [Grant-in-Aid for Scientific Research (A) (11304050)].

References

[1] Gray, G. W., Jones, B., and Marson, F., 1957, *J. chem. Soc*., 393.
[2] Diele, S., and Göring, P., 1998, *Handbook of Liquid Crystals*, Vol. 2B, edited by D. Demus, J. W. Goodby, G. W. Gray, H.-W. Spiess, and V. Vill (Weinheim: Wiley-VCH), p. 887–900.
[3] Schubert, H., Hauschild, J., Demus, D., and Hoffmann, S., 1978, *Z. Chem.*, **18,** 256.
[4] Demus, D., Gloza, A., Hartung, H., Hauser, A., Rapthel, I., and Wiegeleben, A., 1981, *Cryst. Res. Technol.*, **16,** 1445.
[5] Göring, P., Diele, S., Fischer, S., Wiegeleben, A., Pelzl, G., Stegemeyer, H., and Thyen, W., 1998, *Liq. Cryst.*, **25,** 467.
[6] Luzzati, V., and Spegt, A., 1967, *Nature*, **215,** 701.
[7] Tardieu, A., and Billard, J., 1976, *J. Phys. (Paris) Coll.*, **37,** C3–79.
[8] Etherington, G., Leadbetter, A. J., Wang, X. J., Gray, G. W., and Tajbakhsh, A., 1986, *Liq. Cryst.*, **1,** 209.
[9] Levelut, A.-M., and Fang, Y., 1991, *Colloq. Phys.*, **23,** C7–229.
[10] Levelut, A.-M., and Clerc, M., 1998, *Liq. Cryst.*, **24,** 105.
[11] Morimoto, N., Saito, K., Morita, Y., Nakasuji, K., and Sorai, M., 1999, *Liq. Cryst.*, **26,** 219.
[12] Saito, K., Sato, A., Morimoto, N., Yamamura, Y., and Sorai, M., 2000, *Mol. Cryst. liq. Cryst.*, **347,** 249.
[13] Saito, K., Shinhara, T., and Sorai, M., 2000, *Liq. Cryst.*, **27,** 1555.
[14] Maeda, Y., Cheng, G.-P., Kutsumizu, S., and Yano, S., 2001, *Liq. Cryst.*, **28,** 1785.
[15] Maeda, Y., Morita, K., and Kutsumizu, S., 2003, *Liq. Cryst.*, **30,** 157.
[16] Maeda, Y., and Kanetsuna, H., 1985, *Bull. Res. Inst. Polym. Tex*., **149**, 119; Maeda, Y., 1990, *Thermochim. Acta*, **163**, 211.
[17] Maeda, Y., and Koizumi, M., 1996, *Rev. sci. Instrum.*, **67,** 2030.
[18] Saito, K., and Sorai, M., 2002, *Chem. Phys. Lett.*, **366,** 56.
[19] Sato, A., Yamamura, Y., Saito, K., and Sorai, M., 1999, *Liq. Cryst.*, **26,** 1185.
[20] Saito, K., Shinhara, T., Nakamoto, T., Kutsumizu, S, Yano, S., and Sorai, M., 2002, *Phys. Rev. E*, **65,** 031719.
[21] Yamaguchi, T., Yamada, M., Kutsumizu, S., and Yano, S., 1995, *Chem. Phys. Lett.*, **240,** 105.
[22] Kutsumizu, S., Yamaguchi, T., Kato, R., and Yano, S., 1999, *Liq. Cryst.*, **26,** 567.
[23] Saito, K., Sato, A., and Sorai, M., 1999, *Liq. Cryst.*, **25,** 525.
[24] Sorai, M., and Saito, K., 2003, *Chem. Rec.*, **3,** 29.